Fabrication and magnetic characterization of arrays of perpendicular spin valves in the sub-50 nm regime

1. Introduction

The impressive advances in the physics of spin-dependent magnetotransport have favoured the development of new technologies employing magnetoresistive (MR) devices called ‘metallic spin-valves’ and ‘tunnel spin-valves’, whose functioning principle, depending on the physical phenomenon, is based on giant magnetoresistance (GMR) and tunneling magnetoresistance (TMR), respectively [1]. An important example of such emerging technologies is provided by the non-volatile Magnetic Random Access Memories (MRAMs), consisting of an array of spin-valve cells, each one representing a bit of stored data [2] (figure 1).

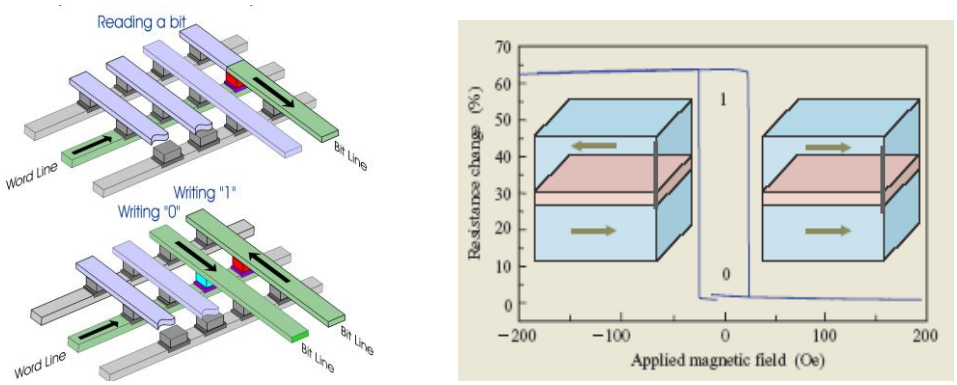

Figure 1. Scheme of the MRAM basic functioning

A basic spin-valve is composed of two ferromagnetic (FM) layers separated by a non-magnetic spacer (NM), metallic in the GMR-based device and insulating in the TMR-based one. One of the two FM films (free layer, FL) is magnetically softer than the other one (reference layer, RL), whose magnetization is pinned through the exchange coupling at the interface with an adjacent antiferromagnetic (AF) layer. Alternatively, the RL can be exchange coupled to a hard ferromagnet, which confers the stability through the soft/hard interface exchange coupling (*pseudo* spin valves – PSV –). In both cases, an external magnetic field will be able to change the orientation of the magnetization of the FL with respect to that of the RL and the resistance of the whole system will vary because of the spin-dependent conductivity effect. The larger the difference between the coercivity (H_c) of FL and RL the larger is the field range where the spin valve operates. Indeed, in order to optimize the performances of spin valves, to achieve a strict control on H_c of FL and RL and on the magnetization reversal process is mandatory.

Nowadays, the increasing demand for miniaturization of magnetic devices triggers an increasing interest in the study of the magnetic properties of elements size-confined to the nanoscale (dots). Fundamental problems may arise that are strictly connected to the magnetic anisotropy and that are collected through the general expression ‘magnetic stability issue’. As the size of the magnetic dots are reduced below a critical value, which depends on the magnetic anisotropy, the magnetization may become unstable against thermal fluctuations, eventually leading to the superparamagnetic state, where H_c vanishes. This effect is definitely detrimental for the right functioning of the spin valve and, ultimately, imply the need of tailoring the magnetic anisotropy of the two FM electrodes.

In this project, the interface exchange coupling was exploited as a tool to tune the effective anisotropy and the macroscopic magnetic properties (magnetization configuration, coercivity, magnetization reversal process and thermal stability) of hard/soft magnetic phases in view of their application as reference and free layer in spintronics devices.

2. Experimental activity

The research activity was devoted to the fabrication of PSV systems in which both the RL and the FL are made of exchange-coupled soft-FM/hard-FM phases with perpendicular anisotropy.
For this purpose a bcc FeCo alloy was used as the soft component, being this phase usually employed in in-plane-anisotropy spin-valves as it provides the highest magnetoresistive response [3]. In order to impose a perpendicular orientation of the magnetization vector, the CoFe component was exchange-coupled to a $[Pt(Pd)/Co]_n$ multilayer structure, which plays the role of the hard phase. This layer consists of *n* repetitions of the Pt(Pd)/Co bilayer structure and shows a perpendicular anisotropy (0.3 ÷ 0.5 MJ/m^3 and 0.5 ÷ 1.2 MJ/m^3 for the $[Pt/Co]_n$ [4] and $[Pd/Co]_n$ [5] system, respectively), originating from the Pt(Pd)/Co interface, whose magnitude can be modulated by varying the thickness and the number *n* of layers [4-8]. The magnetic behaviour of the FeCo/$[Pt(Pd)/Co]_n$ structure was tailored by changing the both the parameters that govern the magnetic properties of the hard component and the thickness of the soft FeCo phase, in order to obtain a structure suitable for the RL (higher anisotropy) or the FL (lower anisotropy) electrodes. $[Pt(Pd)/Co]_n$/FeCo/NM/FeCo/$[Pt(Pd)/Co]_n$ stacks were finally grown by selecting the two-phase structures most suitable to act as RL and FL. With regards to the non-magnetic spacer, the original choice of using an MgO insulating spacer has been temporarily abandoned because of the too large time required to obtain a continuous, stoichiometric and structurally ordered layer and a metallic Cr spacer whose chosen to prepare GMR PSVs.
Continuous $[Pt(Pd)/Co]_n$ films, FeCo/$[Pt(Pd)/Co]_n$ bilayers and $[Pt(Pd)/Co]_n$/FeCo/NM/FeCo/$[Pt(Pd)/Co]_n$ PSV films stacks were deposited at room temperature by dc magnetron sputtering according to the experimental conditions reported in table 1. During the deposition the nominal thickness was monitored using a quartz micro balance, which was calibrated by x-ray reflectometry measurements on single element metallic films. Both thermally oxidized SiO_2/Si(100) and high conductive Si (100) substrates were used, the latter making the subsequent nano-pattering process by electron and focus ion beam lithography more effective. Deposition on pre-patterned mask were not performed as previous results showed a significant deterioration of the magnetic properties when the lift-off procedure is adopted. A preliminary magnetic and magnetotrasport characterization was also carried-out.

Table 1. Sample list.

Sample ID	Seed Layer (Å)	Under Layer (Å)	Hard Layer-1 (Å)	Soft Layer-1 (Å)	Capped Layer / Spacer (Å)	Soft Layer-2 (Å)	Hard Layer-2 (Å)
$[Pt/Co]_n$							
CH2144	Ta (15)	Pt (22)	$[Pt(8)/Co(4)]_4$ P_{Ar} = 10 µbar		Pt(30)		
CH2145	Ta (15)	Pt (22)	$[Pt(8)/Co(4)]_4$ P_{Ar} = 3.5 µbar		Pt(30)		
CH2147	Ta (15)	Pt (22)	$[Pt(8)/Co(6)]_4$ P_{Ar} = 3.5 µbar		Pt(30)		
CH2148	Ta (15)	Pt (22)	$[Pt(8)/Co(6)]_4$ P_{Ar} = 10 µbar		Pt(30)		

$[Pt/Co]_n$/FeCo							
CH2149	Ta (15)	Pt (22)	$[Pt(8)/Co(4)]_4/Pt(8)$ P_{Ar} = 10 µbar	FeCo(6)	Pt(30)		
CH2150	Ta (30)	Pt (22)	$[Pt(8)/Co(4)]_4/Pt(8)$ P_{Ar} = 10 µbar	FeCo(10)	Pt(30)		
CH2152	Ta (30)	Pt (22)	$[Pt(8)/Co(4)]_4/Pt(8)$ P_{Ar} = 10 µbar	FeCo(20)	Pt(30)		
CH2151	Ta (30)	Pt (22)	$[Pt(8)/Co(6)]_4/Pt(8)$ P_{Ar} = 3.5 µbar	FeCo(6)	Pt(30)		
$[Pt/Co]_n$/FeCo/Cu/FeCo/$[Pt/Co]_n$							
CH2156	Ta (30)	Pt (22)	$[Pt(8)/Co(6)]_4/Pt(8)$ P_{Ar} = 3.5 µbar	FeCo(6)	Cu(18)	FeCo(6)	$[Pt(8)/Co(4)]_4/Pt(30)$ 10 µbar
$[Pd/Co]_n$							
CH2160	Ta (30)	Pd (22)	$[Pd(\mathbf{8})/Co(\mathbf{4})]_4$ P_{Ar} = 3.5 µbar		Pd(30)		
CH2161	Ta (30)	Pd (21)	$[Pd(\mathbf{9})/Co(\mathbf{3})]_4$ P_{Ar} = 3.5 µbar		Pd(30)		
CH2162	Ta (30)	Pd (21)	$[Pt(\mathbf{9})/Co(\mathbf{3})]_8$ P_{Ar} = 10 µbar		Pd(30)		
$[Pd/Co]_n$/FeCo							
CH2168	Ta (30)	Pd (22)	$[Pd(\mathbf{8})/Co(\mathbf{4})]_4/Pd(\mathbf{8})$ P_{Ar} = 3.5 µbar	FeCo(**6**)	Pd(30)		
CH2163	Ta (30)	Pd (21)	$[Pd(\mathbf{9})/Co(\mathbf{3})]_4/Pd(\mathbf{9})$ P_{Ar} = 10 µbar	FeCo(**6**)	Pd(30)		
CH2164	Ta (30)	Pd (21)	$[Pd(\mathbf{9})/Co(\mathbf{3})]_4/Pd(\mathbf{9})$ P_{Ar} = 3.5 µbar	FeCo(**6**)	Pd(30)		
CH2169	Ta (30)	Pd (21)	$[Pd(\mathbf{9})/Co(\mathbf{3})]_4/Pd(\mathbf{9})$ P_{Ar} = 3.5 µbar	FeCo(**10**)	Pd(30)		
$[Pd/Co]_n$/FeCo/Cu/FeCo/$[Pd/Co]_n$							
CH2166	Ta (30)	Pd (22)	$[Pd(\mathbf{8})/Co(\mathbf{4})]_4/Pd(\mathbf{8})$ P_{Ar} = 3.5 µbar	FeCo(**6**)	Cu(**21**)	FeCo(**6**)	$[Pd(\mathbf{9})/Co(\mathbf{3})]_4/Pd(30)$ P_{Ar} = 3.5 µbar
CH2167	Ta (30)	Pd (22)	$[Pd(\mathbf{8})/Co(\mathbf{4})]_4/Pd(\mathbf{8})$ P_{Ar} = 3.5 µbar	FeCo(**6**)	Cu(**51**)	FeCo(**6**)	$[Pd(\mathbf{9})/Co(\mathbf{3})]_4/Pd(30)$ P_{Ar} = 3.5 µbar

2.1. $[Pt(Pd)/Co]_n$ films

$[Pt(Pd)/Co]_n$ films were prepared by varying both the sputter gas (Ar) pressure and the layer thickness ratio to obtain magnetic films with a hard but different perpendicular magnetic anisotropy constant (and coercivity) to be used as the hard part of the reference and free layers.

Room temperature perpendicular and in-plane magnetization curves of $[Pt/Co]_n$ films are reported in figure 2 and 3. All the samples are characterized by a squared perpendicular hysteresis loop and an in-plane magnetization curve with a vanishing coercivity and remanence, consistent with a perpendicular easy-axis. The effective magnetic anisotropy constant values (K_{eff}), evaluated from the area enclosed between the two curves, are collected in table 2 together with the perpendicular coercivity ($H_{c,\perp}$) and the saturation magnetization (M_s). Samples CH2144 and CH2147 (K_{eff} ~ 0.45 and 0.20 MJ/m^3, respectively) were chosen for the hard component of the RL and FL, respectively and will be referred hereafter as and , where the apices *H* and *L* stand for *higher* and *lower* anisotropy.

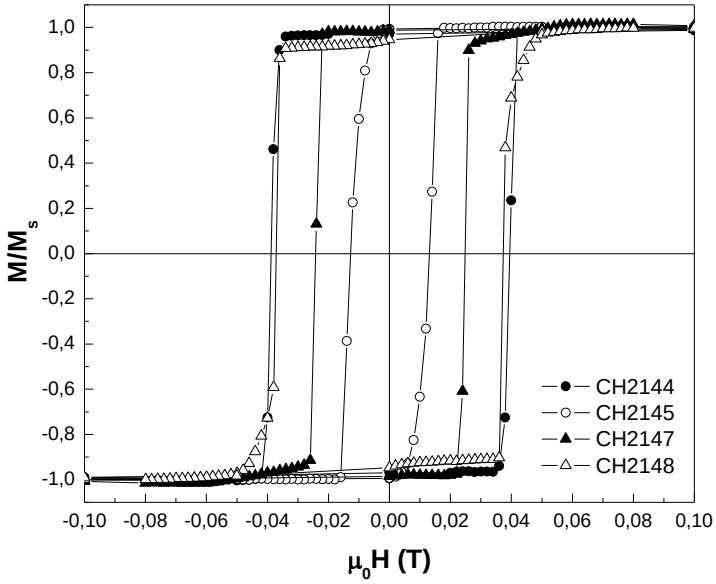

Figure 2. Room temperature perpendicular hysteresis loops of $[Pt/Co]_n$ films as a function of the Ar pressure and Pt/Co thickness ratio.

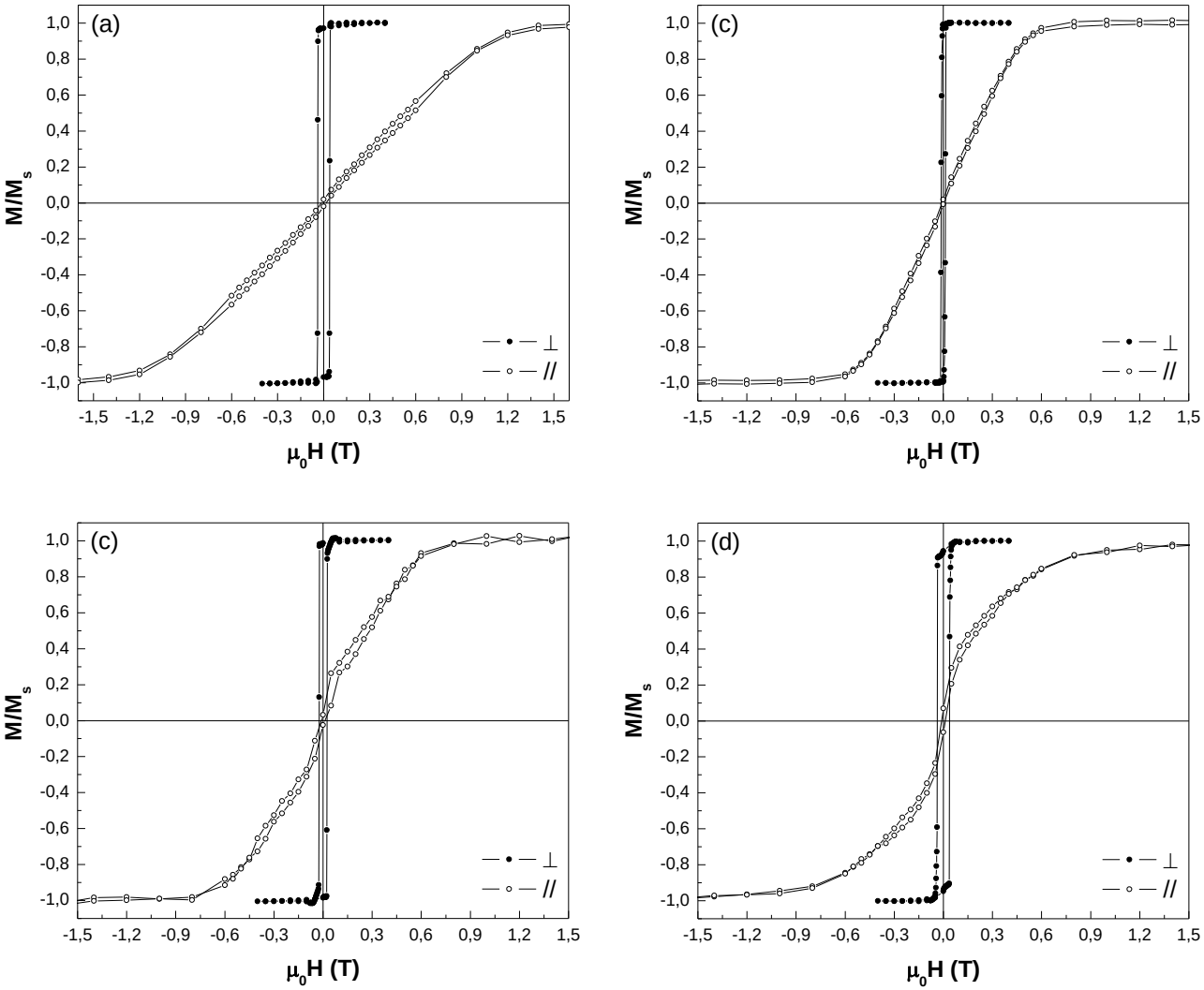

Figure 3. Room temperature perpendicular (⊥) and in-plane (//) magnetization curves of $[Pt/Co]_n$ films as a function of the Ar pressure and Pt/Co thickness ratio. (a) Sample CH2144; (b) sample CH2145; (c) sample CH2147; (d) sample CH2148.

Room temperature perpendicular and in-plane magnetization curves of $[Pd/Co]_n$ films are reported in figure 4 and 5. All the samples are characterized by a squared perpendicular hysteresis loop and an in-plane magnetization curve with a vanishing coercivity and remanence, consistent with a perpendicular easy-axis. The magnetic anisotropy constant values are collected in table 2 together with the perpendicular coercivity and the saturation magnetization. Samples CH2161 and CH2160 (K_{eff} ~ 0.55 and 0.47 MJ/m^3, respectively) were chosen for the hard component of the RL and FL, respectively. As expected, using Pd instead of Pt allows the magnetic anisotropy to be increased. Hereafter the two samples will be referred as and , where the apices *H* and *L* stand for *higher* and *lower* anisotropy.

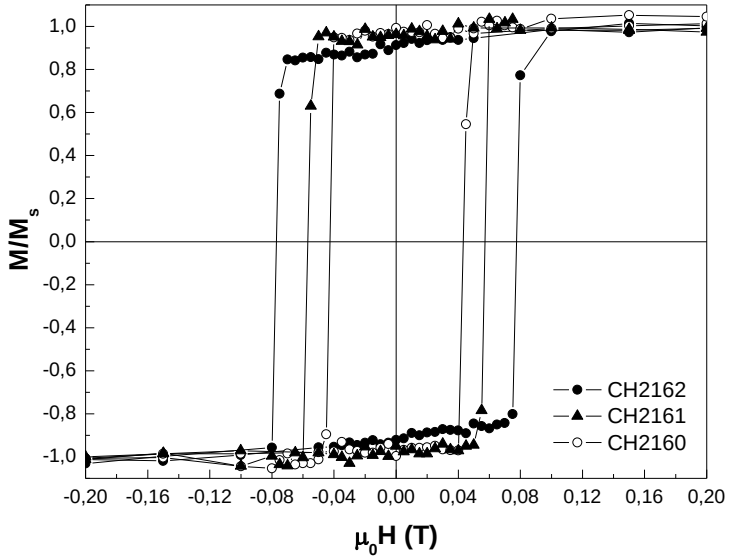

Figure 4. Room temperature perpendicular hysteresis loops of $[Pd/Co]_n$ films as a function of the Ar pressure and Pd/Co thickness ratio.

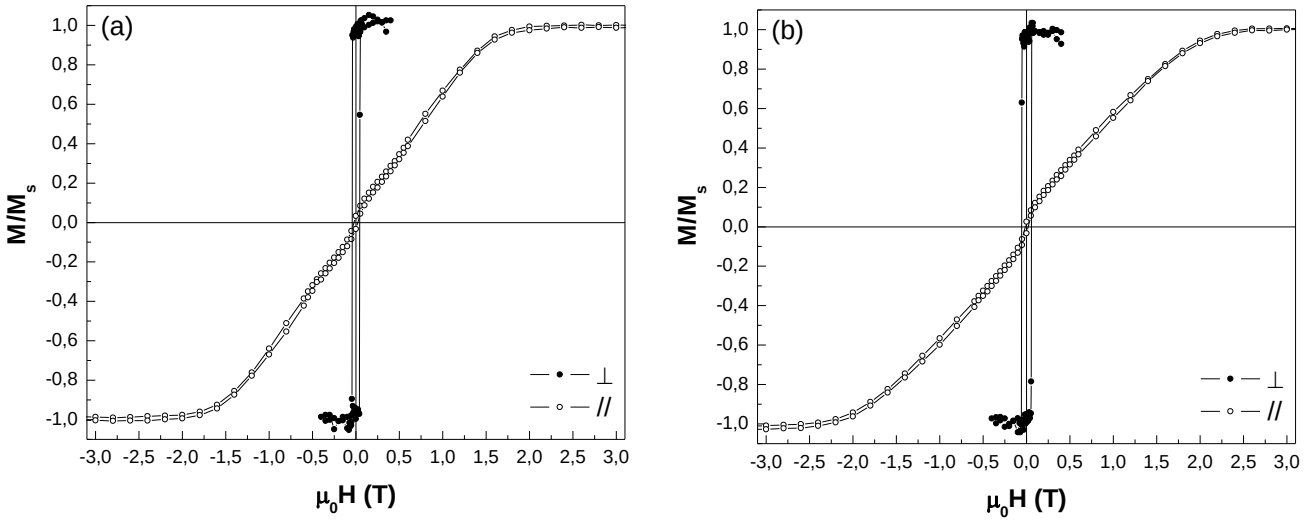

Figure 5. Room temperature perpendicular (⊥) and in-plane (//) magnetization curves of $[Pd/Co]_n$ films as a function of the Ar pressure and Pd/Co thickness ratio. (a) Sample CH2160; (b) sample CH2161.

Table 2. Room temperature magnetic properties (K_{eff}, $H_{c,\perp}$ and M_s) of $[Pt/Co]_n$ and $[Pd/Co]_n$ samples determined from the perpendicular and in-plane magnetization curves.

Sample ID	$H_{c,\perp}$ (mT)	M_s (kA/m)	K_{eff} (MJ/m^3)
$[Pt/Co]_n$			
CH2144	~38	~690	~0.45
CH2145	~13	~500	~0.15
CH2147	~24	~780	~0.20
CH2148	~37	~980	~0.35
$[Pd/Co]_n$			
CH2160	~43	~670	~0.47
CH2161	~57	~570	~0.55

2.2. FeCo/$[Pt(Pd)/Co]_n$ films

Soft/Hard bilayers with a FeCo thickness in the range of 6 and 20 Å were prepared to individuate the maximum thickness that still guarantees a perpendicular orientation of the magnetization vector in the soft phase. It is worth mentioning that the thickness of the FeCo phase must be as large as possible to enhance the spin polarization of the current in a PSV stack. The $[Pt(Pd)/Co]_n$ films selected in the previous analysis were used as the hard phase.

Room temperature perpendicular magnetization curves of FeCo/$[Pt/Co]_n$ bilayers are reported in figure 6 as a function of the soft layer thickness. The perpendicular hysteresis loops of the hard layer is also reported for comparison. Using the hardest phase allows the perpendicular alignment of the moments in the hard and soft layers to be almost obtained for a FeCo thickness of 6 Å, as indicated by the slightly decrease of the perpendicular normalized remanence (figure 6a). Increasing the soft layer thickness causes a steadily reduction of the perpendicular normalized remanence, which suggests a tilting of the magnetization of the soft layer towards the in-plane direction, due to the competition between the shape anisotropy and the interface exchange-coupling [9]. When a hard layer with a lower anisotropy is used (figure 6b) a worsening of the out-of-plane alignment of the soft and hard moments is observed even for a CoFe thickness of 6 Å. Although a perfect out-of-plane alignment was not observed in both the bilayers, samples CH2149 and CH2152 (with a 6 Å thick FeCo layer), which show a different perpendicular coercivity – ~35 and ~19 mT, respectively – (figure 7), were chosen as the reference and free layer of the PSV stack, respectively.

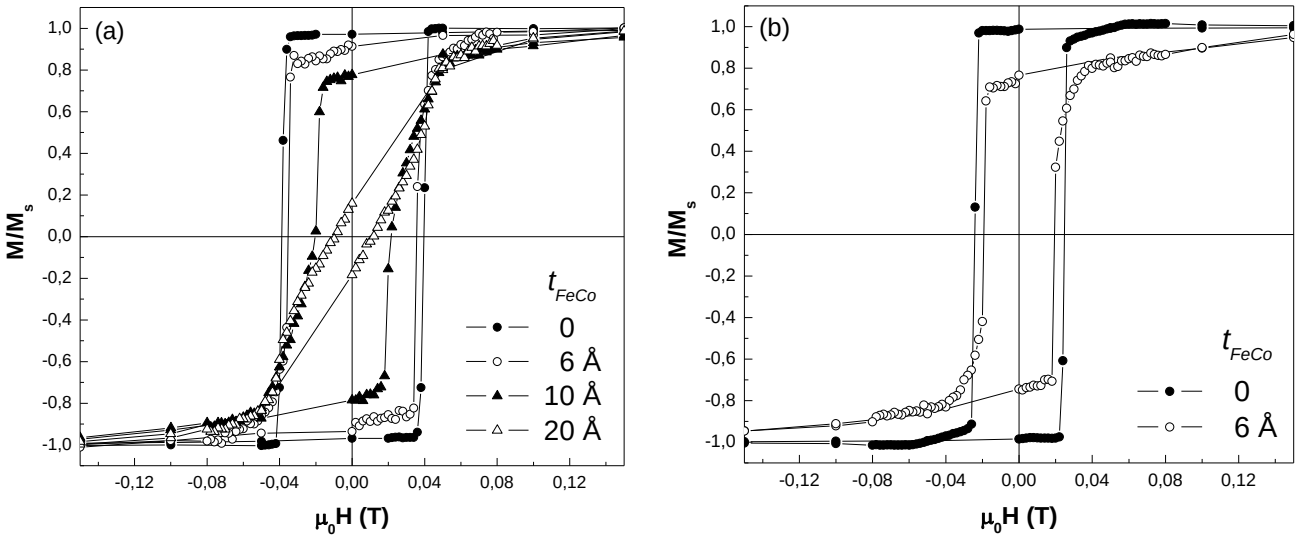

Figure 6. Room temperature perpendicular hysteresis loops of (a) FeCo/ and FeCo/ bilayers as a function of the FeCo soft layer thickness (t_{FeCo}). The perpendicular hysteresis loops of the hard layer is also reported for comparison.

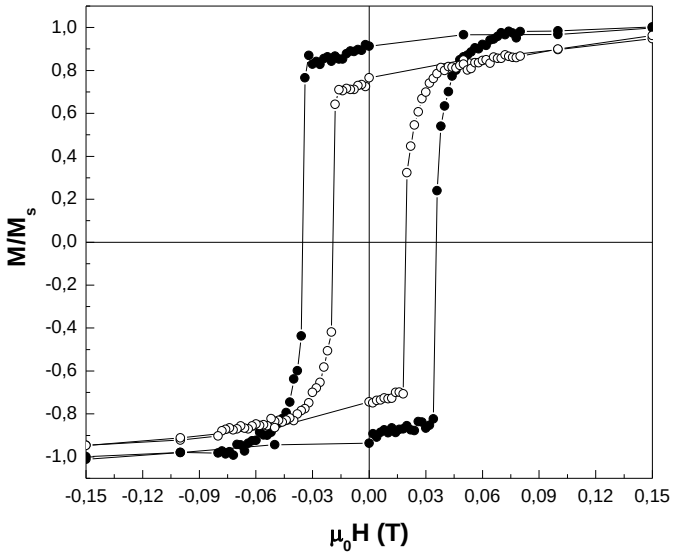

Figure 7. Comparison of room temperature perpendicular hysteresis loops of FeCo(6Å)/ (– ● –) and FeCo(6Å)/ (– ○ –) bilayers.

When a $[Pd/Co]_n$ layer is used as the hard phase, a perfect out-of-plane alignment between soft and hard moments is observed for a FeCo thickness of 6Å for both FeCo/ and FeCo/ bilayers due to the larger anisotropy of the $[Pd/Co]_n$ system (figure 8). In other words a rigid exchange-coupled system, consisting of hard and soft phase with perpendicular anisotropy was obtained [9]. Differently to the FeCo/$[Pt/Co]_n$ system, a almost perpendicular magnetization in the soft layer is also obtained for a FeCo thickness of 10Å due to the larger anisotropy of the $[Pd/Co]_n$ system. Samples CH2161 and CH2168 (with a 6 Å thick CoFe layer), showing a different perpendicular coercivity – ~38 and ~11 mT, respectively – (figure 9), were chosen as the reference and free layer of the PSV stack, respectively.

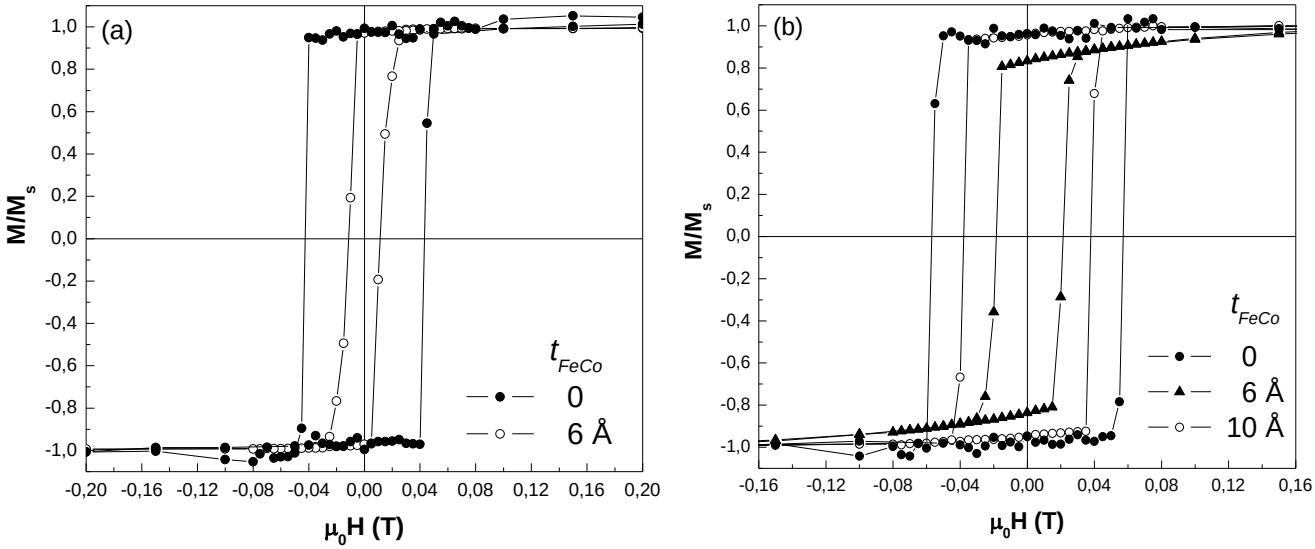

Figure 8. Room temperature perpendicular hysteresis loops of (a) FeCo/ and (b) FeCo/ bilayers as a function of the FeCo soft layer thickness (t_{FeCo}). The perpendicular hysteresis loops of the hard layer is also reported for comparison.

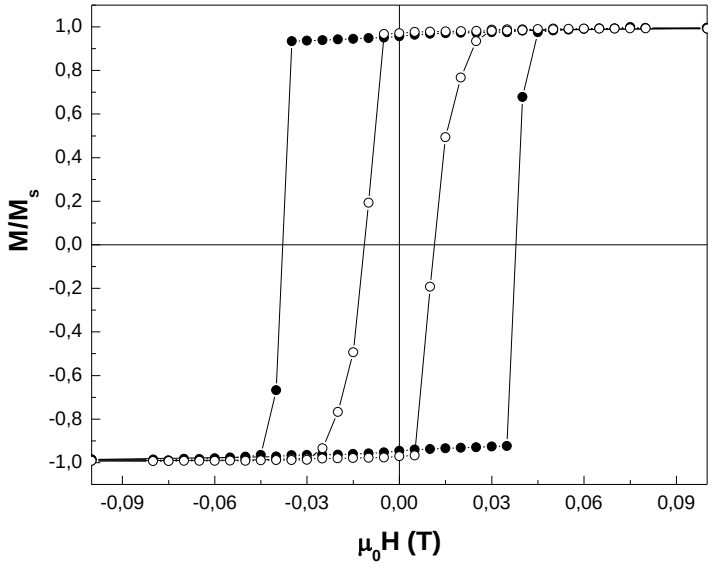

Figure 9. Comparison of room temperature perpendicular hysteresis loops of CoFe(6Å)/ (– ● –) and CoFe(6Å)/ (– ○ –) bilayers.

In figure 10 the perpendicular hysteresis loops of CoFe(10Å)/ bilayers deposited on SiO_2/Si(100) and high conductive Si(100) substrates are reported to demonstrate that the same magnetic properties are obtained independently of the substrate.

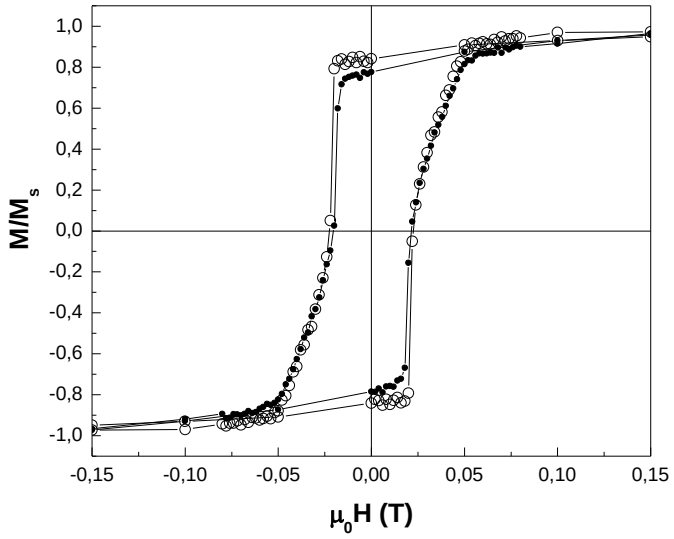

Figure 10. Comparison of room temperature perpendicular hysteresis loops of FeCo(10Å)/ bilayers deposited on SiO_2/Si(100) (– ● –) and high conductive Si(100) (– ○ –) substrates.

2.3. /FeCo(6Å)/Cu/FeCo(6Å)/ PSV film stacks

On the basis of previous results, /FeCo(6Å)/Cu/FeCo(6Å)/ PSV film stacks were deposited using a thin Cu layer (~ 2 Å) as non-magnetic spacer. For $[Pd/Co]_n$-based PSVs a Cu thickness t_{Cu} ~ 5Å was also used.

Room temperature perpendicular hysteresis loops of the three samples are reported in figure 11(left panel). The behaviour of the PSVs film stack is not a simple superposition of the hysteresis loops of the individual reference and free layers (as expected for ideal PSV stacks), the overall shape suggesting a strong dipolar coupling between the constituent layers across the Cu spacer leading to a vertically correlated domains through the whole film stack [10 - 12]. Reducing the measurement temperature down to 5 K (figure 11- left panel), seems to indicate a partial decoupling for the [Pd/Co]-based PSV film stacks, this effect being larger in the sample with a larger Cu thickness. At low temperature, the coercivity of the reference layer increases to a point where the stray field emanating from the free layer could be less effective in supporting its reversal. For the [Pt/Co]-based PSV film stack, the two layers are still strongly coupled even at low temperature likely due to the lower anisotropy (and coercivity) of the [Pt/Co]-based RL.

When the samples will be nanopatterned to a size below the single domain threshold (e.g. 200 nm for $[Pd/Co]_n$ [13]) an increase of coercvity of the $[Co/Pt(Pd)]_n$ layer is expected, which could result in a change of the coupling between the layers.

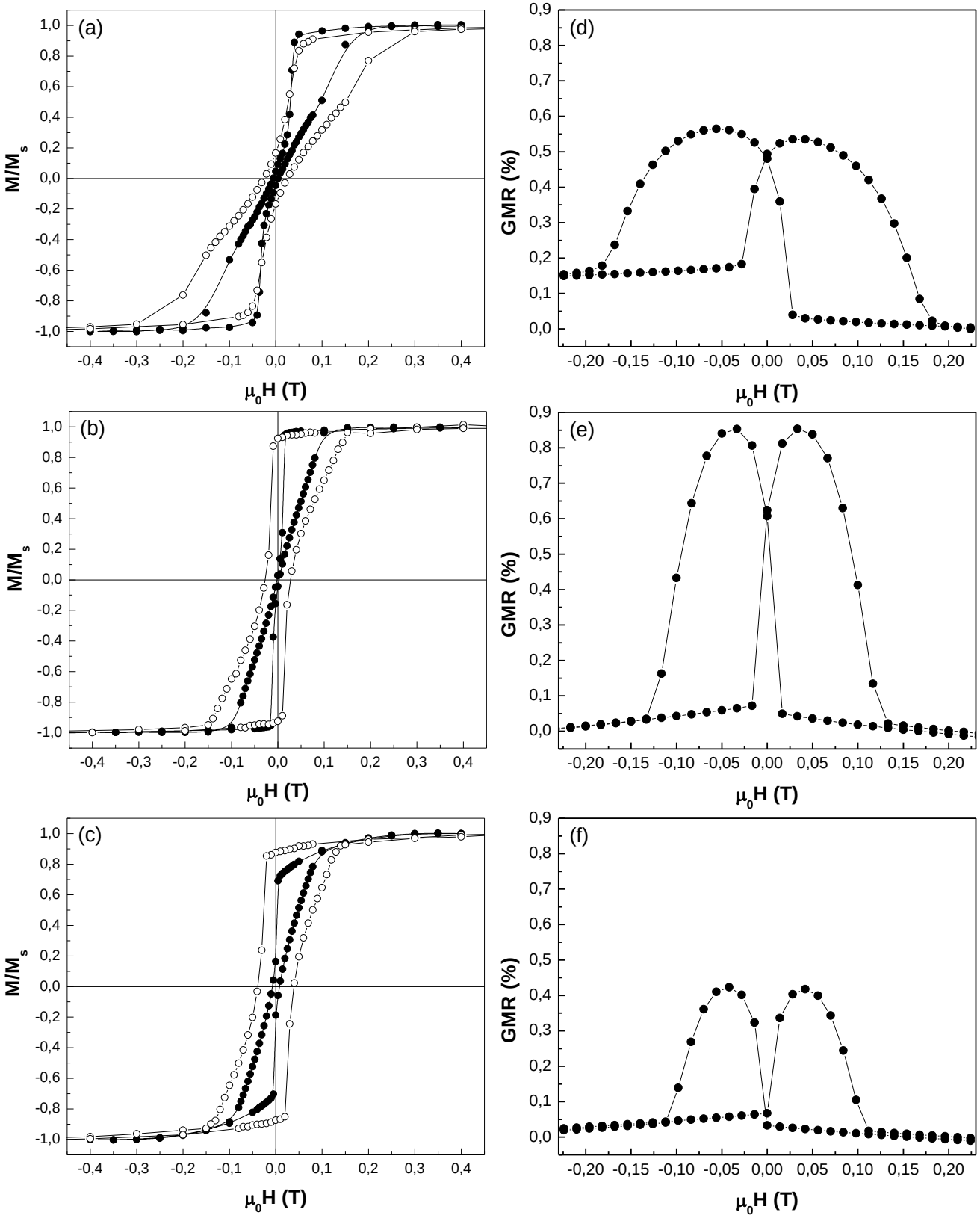

Figure 11. (Left) Room (– ● –) and low (5K, – ○ –) temperature perpendicular magnetization curves of /CoFe(6Å)/Cu/CoFe(6Å)/ PSV stacks. (Right) Corresponding room temperature magnetoresistance curves. (a,d) Hard phase: $[Co/Pt]_n$, t_{Cu} = 1.8 Å ; (b,e) Hard phase: $[Co/Pd]_n$, t_{Cu} = 2.1 Å ; (c,f) Hard phase: $[Co/Pd]_n$, t_{Cu} = 5.1 Å.

Room temperature magnetotransport properties were measured by a four-point probe method in current-in-plane geometry with the external field applied perpendicular to the sample surface (figure 11 – right panel). All plotted curves have a parabolic R(H) dependence with a large hysteresis, typical for PVS systems with vertically correlated domains [10,12]. Keeping constant the Cu thickness (~2 Å), an increase of GMR ratio from ~0.55 % to ~0.85% was found by moving from a [Pt/Co]- to a [Pd/Co]-based PSV film stack. Increasing the Cu thickness up to ~5 Å leads to a degradation of the maximum resistance change (~0.45 %) due to laminar- like currents not giving rise to the GMR effect.

3. Perspectives

- Room temperature angular magnetic measurements are in progress to carefully investigate the magnetization reversal mechanism and the magnetization easy axis arrangement.
- Focused ion beam lithography is in progress to investigate the effect of nano-patterning on the magnetic properties. Samples will be characterized by MOKE magnetometer and MFM microscopy.
- Electron beam lithography will be carried out on selected samples to produce large area dots arrays for angular magnetic measurements.

References

[1] M. N. Baibich *et al.*, *Phys. Rev. Lett.* 61, 2472 (1988)
[2] J. Akerman, *Science 308*, 508 (2005)
[3] S.S.P. Parkin *et al.*, *Nature Mater.* 3, 862 (2004)
[4] D. Makarov *et al.*, *Appl. Phys. Lett.* 96, 062501 (2010)
[5] B. J. Kirby *et al.*, J. *Appl. Phys.* 117, 063905 (2015)
[6] M.T. Johnson *et al.*, *Rep. Prog. Phys.* 59, 1409 (1996)
[7] H.H.G. Draaisma *et al.*, *J. Magn. Magn. Mater.* 66, 351 (1987)
[8] G.C. Lin *et al.*, *J. Magn. Magn. Mater.* 93, 194 (1991)
[9] G. Varvaro *et al.*, *New J. Phys.* 14, 073008 (2012)
[10] P. Mathhes *et al.*, *IEEE trans. Magn.* 51, 4400104 (2015)
[11] S.M. Mohseni *et al.*, *Phys. Rev. B* 84, 174432 (2011)
[12] J.E. Davies *et al.*, *Appl. Phys. Lett.* 103, 022409 (2013)
[13] T. Thomson *et al.*, *Phys. Rev. Lett.* 96, 257204 (2006)